Trajectory Studies of S_N2 Nucleophilic Substitution. 7. $F^- + CH_3Cl \rightarrow FCH_3 + Cl^-$

Timothy Su*

Department of Chemistry, University of Massachusetts, N. Dartmouth, Massachusetts 02747-2300

Haobin Wang† and William L. Hase*

Department of Chemistry, Wayne State University, Detroit, Michigan 48202-3489

Received: May 27, 1998; In Final Form: September 18, 1998

The PES(F,Cl) analytic potential energy surface, developed previously, is used in a trajectory study of the $F^- + CH_3Cl$ S_N2 reaction. The trajectory S_N2 rate constants, as a function of reactant relative translational energy E_{rel} and CH_3Cl temperature, are in good overall agreement with the experimental rate constants and those calculated using an ion−molecule capture/RRKM statistical model applied to PES(F,Cl). The latter agreement exists even though the reaction dynamics is decidedly nonstatistical. For high E_{rel} the reaction is direct. At lower E_{rel} there is evidence for formation of an ion−molecule complex; however, its lifetime is too short for complete energy randomization to occur. The velocity scattering angle is isotropic at low E_{rel} but becomes anisotropic with forward scattering as E_{rel} is increased. The reaction exothermicity is primarily partitioned to product vibration, in disagreement with a previous experimental study. Energy transfer from the reactants to products is very selective. Excess reactant relative translational energy almost exclusively goes to product relative translation. Similarly, C−Cl stretch excitation goes to product vibration. For a 300 K CH_3Cl rotational temperature, the total angular momentum is dominated by the reactant orbital angular momentum, which is strongly correlated with the product orbital angular momentum.

I. Introduction

There is considerable interest, both experimentally[1−22] and theoretically,[23−42] in gas-phase S_N2 nucleophilic substitution reactions of the type

$$X^- + CH_3Y \rightarrow XCH_3 + Y^- \quad (1)$$

Potential energy surfaces for this class of reactions are comprised of a central barrier which separates the potential minima for the two ion−molecule complexes X^-- - -CH_3Y and XCH_3- - -Y^-. Statistical theories such as Rice−Ramsperger−Kassel−Marcus (RRKM),[43] phase space theory (PST),[43] and transition state (TST)[44] theory have been widely used to model kinetics of S_N2 reactions. However, the results of several recent experimental studies of S_N2 reactions are not adequately explained by these theories.[8,13,18,19,22,33,40] Classical trajectory simulations[24,27,29,30,32,41] have proven very useful for interpreting the kinetics and dynamics of S_N2 reactions and have brought into question fundamental assumptions of statistical theories regarding mode specific chemistry, intramolecular vibrational energy redistribution (IVR), and the dynamics of central barrier crossing.

The following family of S_N2 reactions

$$F^- + CH_3Cl \rightarrow FCH_3 + Cl^- \quad (2)$$

$$F^- + CH_3Br \rightarrow FCH_3 + Br^- \quad (3)$$

$$F^- + CH_3I \rightarrow FCH_3 + I^- \quad (4)$$

are of particular interest because of their large reaction exothermicity and small central barrier with respect to the F$^-$- - -CH_3X potential energy minimum.[4,7a,16,36,40,42] Ab initio energies[36,40,42] for stationary points on the $F^- + CH_3Cl \rightarrow FCH_3 + Cl^-$ potential energy surface are listed in Table 1. The calculations at the highest level of theory are those performed by Botschwina and co-workers[42] with the CCSD(T) method, which give a [F- -CH_3- -Cl]$^-$ central barrier energy of −12.75 kcal/mol with respect to the reactants, a reaction exothermicity of −32.92 kcal/mol, and a F$^-$- - -$CH_3Cl \rightarrow$ [F- -CH_3- -Cl]$^-$ unimolecular barrier of 3.05 kcal/mol. After considering basis set superposition error (BSSE) and additional electron correlation and basis set effects, Botschwina and co-workers[42] recommend 3.3 ± 0.3 kcal/mol for the unimolecular barrier. A best

TABLE 1: Energies for $F^- + CH_3Cl \rightarrow FCH_3 + Cl^-$ Stationary Points[a]

	stationary point			
theory	F$^-$- - -CH_3Cl	[F- -CH_3- -Cl]$^-$	FCH_3- - -Cl^-	$FCH_3 + Cl^-$
MP2[b]	−15.80	−11.56	−41.20	−31.32
QCISD[b]	−16.08	−12.48	−44.10	−34.61
QCISD(T)[b]	−16.56	−13.95	−43.44	−33.54
G2(+)[c]	−15.60	−12.62	−41.06	−31.42
MP2[d]	−14.92	−10.40	−39.59	−29.95
CCSD[d]	−15.25	−11.02	−43.79	−34.61
CCSD-T[d]	−15.77	−12.62	−42.60	−33.01
CCSD(T)[d]	−15.80	−12.75	−42.53	−32.92
PES(F,Cl)[e]	−15.83	−11.56	−41.23	−31.32

[a] Energies, with respect to the reactants $F^- + CH_3Cl$, are in kcal/mol and do not include zero-point energies. [b] Calculations from ref 40 with the 6-311++G(2df,2pd) basis set. Geometries were optimized at the MP2 level of theory. [c] Reference 35(b). [d] Calculations from ref 42 with a basis set consisting of 289 contracted Gaussian-type orbitals (cGTOs). Geometries were optimized at the same level of theory but with a basis consisting of 244 cGTOs. [e] The analytic potential energy function, from ref 40, used for the trajectory results presented here.

† Current address: Department of Chemistry, University of California, Berkeley, CA 94720.

10.1021/jp982386u CCC: $15.00
Published on Web 11/10/1998

value of −31.5 kcal/mol is obtained for the 298 K reaction exothermicity, after including zero-point and thermal energy differences between the reactants and products.[42] This reaction exothermicity is in good agreement with the experimental values of −31[7a] and −34.3 ±1 kcal/mol.[45]

The rate constants for reactions 2 and 3 have been measured at 300 K[7a,16] and found to be smaller than the values predicted by ion−molecule capture.[46,47] In a more dynamical study,[4] the rate constants for reactions 2−4 were measured versus relative translational energy and CH_3X temperature in variable temperature-selected ion flow drift tube (VT-SIFDT) experiments. It was observed that the reaction rate constants are insensitive to the internal (vibrational−rotational) temperature of the polar neutrals but depend on the relative translational energy of the ion−molecule partners. The reaction rate constant for each reaction is lower than the collision limiting value, even for low relative translational energies. The rate constant decreases relatively slowly with increasing energy for energies below 0.2−0.3 eV but decreases more rapidly with increasing energy for higher energies.

To model these experiments, Su et al.[4] used a simple dynamical model that assumes the molecule is a linear dipole and there is an orientation effect for reaction with the probability function

$$P(\theta) = |\cos^n(\theta/2)| \qquad (5)$$

where θ is the collision orientation angle and n is an adjustable parameter. Values for θ of 0 and π correspond to backside and frontal attack, respectively, along the C−X symmetry axis. This simple theoretical approach yields only qualitative agreement with experimental results but does suggest an orientation requirement for reaction to occur. The lack of quantitative agreement with experiment may be due to the model's oversimplified dynamical assumptions and approximate potential. To illustrate the possible need for a more detailed dynamical model, two microscopic reaction mechanisms are found in trajectory simulations of the $Cl^- + CH_3Cl$ S_N2 reaction: direct substitution and indirect substitution via trapping in the ion−molecule complexes.[29] The direct mechanism prefers the orientation angle $\theta = 0$, but since ion−molecule association occurs as a result of translation to rotation energy transfer, nonoriented collisions with θ intermediate of 0 and $\pi/2$ are preferred for the indirect mechanism.

From an experimental study,[9] it was concluded that most of the energy released in reaction 2 is partitioned to product relative translation. It is estimated that the majority of the CH_3F product molecules receive less than 20% of the available energy as vibrational/rotational excitation. This type of energy partitioning is much different than what has been found for Cl^-- - -$CH_3Br \rightarrow ClCH_3 + Br^-$ unimolecular dissociation from both experimental[8] and trajectory[30] studies. Here, very little of the available product energy is released to relative translation and is, instead, primarily partitioned to CH_3Cl vibration.

The multidimensional analytic potential energy function PES-(F,Cl) was derived for $F^- + CH_3Cl \rightarrow FCH_3 + Cl^-$, reaction 2, from MP2/6-311++G(2df,2pd) ab initio calculations and used in statistical ion−molecule capture/RRKM calculations of the reaction rate constant versus CH_3Cl temperature T_{CH_3Cl} and reagent relative translational energy E_{rel}.[40] The calculated rate constant was found to be weakly dependent on T_{CH_3Cl}, in agreement with experiment. However, the decrease in the experimental rate constant with increase in E_{rel} was only semiquantitatively reproduced by the statistical theory calculations. The best fit to the experimental data is achieved with a central barrier energy larger than that found from the ab initio calculations. For example, fitting the room-temperature experimental point with $E_{rel} = 0.9$ kcal/mol and $T_{CH_3Cl} = 296$ K requires a central barrier of −10.36 kcal/mol. From Table 1, it is seen that this fitted barrier is 2.39 kcal/mol higher than the barrier for the CCSD(T) calculations of Botschwina and coworkers.[42]

TABLE 2: Geometries for $F^- + CH_3Cl \rightarrow FCH_3 + Cl^-$ Stationary Points[a]

	R_{C-F}	R_{C-Cl}	R_{C-H}	∠Cl−C−H	∠H−C−H
		$F^- + CH_3Cl$ Reactants			
MP2[b]	∞	1.778	1.083	108.6	110.3
CCSD(T)[c]	∞	1.787	1.086	108.4	110.5
PES(F,Cl)[d]	∞	1.778	1.085	108.9	110.0
		F^-- - -CH_3Cl Complex			
MP2	2.511	1.837	1.077	108.1	110.8
CCSD(T)	2.502	1.853	1.080	107.6	111.2
PES(F,Cl)	2.521	1.831	1.078	108.1	110.8
		[F- - -CH_3- - -Cl]$^-$ Saddle Point			
MP2	1.997	2.106	1.069	95.9	119.0
CCSD(T)	2.030	2.121	1.072	96.3	118.8
PES(F,Cl)	1.995	2.108	1.069	96.1	118.9
		FCH_3- - -Cl^- Complex			
MP2	1.413	3.178	1.082	70.9	109.9
CCSD(T)	1.417	3.188	1.086	71.1	110.1
PES(F,Cl)	1.410	3.198	1.082	70.7	109.7
		$FCH_3 + Cl^-$ Products			
MP2	1.383	∞	1.086	71.1	110.0
CCSD(T)	1.387	∞	1.090	71.3	110.2
PES (F,Cl)	1.383	∞	1.085	70.9	109.8

[a] Distances are in angstroms, angles and in degrees. [b] Calculations from ref 40, with the 6-311++G(2df,2pd) basis set. [c] Calculations from ref 42, with a basis of 244 cGTOs. [d] Analytic potential energy function from ref 40.

The above experimental and statistical rate theory calculations illustrate the need of calculations for $F^- + CH_3Cl \rightarrow FCH_3 + Cl^-$, which probe the reaction dynamics. In this article a classical trajectory study of this reaction, based on the analytic potential energy function PES(F,Cl), is reported. The trajectories are used to calculate (1) the reaction rate constant, (2) orientational effects on the reaction probability, (3) the F^-- - -CH_3Cl and FCH_3- - -Cl^- lifetimes, (4) the effect of mode specific excitation on the reaction mechanism and rate, and (5) product energy, angular momentum, and scattering angle distributions.

II. PES(F,Cl) Analytic Potential

The PES(F,Cl) analytic potential energy function was derived by fitting MP2/6-311++ G(2df,2pd) ab initio calculations.[40] A detailed discussion of PES(F, Cl) was given previously,[40] and only a few of its salient features are discussed here. As shown in Table 1, the stationary point energies for PES(F,Cl) are in good agreement with the highest level ab initio calculations performed with the CCSD(T) method.[42] The [F- -CH_3- -Cl]$^-$ central barrier energy for PES(F,Cl) is only 1.2 kcal/mol higher than the CCSD(T) value. The reaction exothermicity for PES-(F,Cl) is in good agreement with the experimental values.[7a,45]

Geometries and vibrational frequencies for the PES(F,Cl) stationary points are compared with the CCSD(T)[42] and CEPA-1[41,42] values in Tables 2 and 3. The CEPA-1 calculations were performed with a basis of 169 cGTOs, roughly equivalent to the 6-311+G** basis. Overall, the PES(F,Cl) and CCSD(T) geometries are in very good agreement. However, the CCSD-(T) C−Cl and C−F bond lengths at the central barrier are 0.02−0.03 Å larger than the PES(F,Cl) values. This is the most

TABLE 3: Harmonic Frequencies for $F^- + CH_3Cl \rightarrow FCH_3 + Cl^-$ Stationary Points[a]

mode	MP2[b]	CEPA-1[c]	expt.[d]	PES (F,Cl)
		$F^- + CH_3Cl$ Reactants		
A_1, C−Cl str	769	741	751	772
E, CH_3 rock	1042	1043	1037	1029
A_1, CH_3 deform	1397	1397	1396	1490
E, CH_3 deform	1502	1503	1496	1415
A_1, C−H str	3120	3088	3088	3102
E, C−H str	3232	3184	3183	3230
		F- - -CH_3- - -Cl Complex		
E, F^- bend	78	107		79
A_1, F−C str	174	181		172
A_1, C−Cl str	612	560		588
E, CH_3 rock	966	962		1043
A_1, CH_3 deform	1277	1280		1396
E, CH_3 deform	1463	1483		1399
A_1, C−H str	3186	3157		3215
E, C−H str	3317	3273		3361
		Saddle Point		
E, F−C−Cl bend	257	230		229
A_1, F−C−Cl str	305	289		306
E, CH_3 rock	1007	1043		1208
A_1, out-of-plane bend	1151	1159		1280
E, CH_3 deform	1427	1426		1406
A1, C−H str	3224	3202		3224
E, C−H str	3422	3374		3421
reaction ccordinate	501i	401i		498i
		FCH_3- - -Cl^- Complex		
E, Cl^- bend	94	96		92
A_1, C−Cl str	113	109		115
A_1, F−C str	989	982		997
E, CH_3 rock	1165	1162		1176
A_1, CH_3 deform	1446	1449		1627
E, CH_3 deform	1504	1507		1445
A_1, C−H str	3138	3095		3148
E, C−H str	3255	3191		3280
		$FCH_3 + Cl^-$ Products		
A_1, F−C str	1086	1078	1078	1087
E, CH_3 rock	1211	1212	1204	1170
A_1, CH_3 deform	1505	1502	1496	1653
E, CH_3 deform	1521	1511	1515	1441
A_1, C−H Str	3097	3057	3075	3107
E, C−H str	3199	3134	3147	3232

[a] Frequency units are cm^{-1}. [b] Calculations from ref 40, with the 6-311++G(2df,2pd). [c] Calculations from ref 41, with a basis of 169 cGTOs, roughly equivalent to the 6-311+G** basis. [d] The experimental CH_3Cl and CH_3F harmonic frequencies are from refs 48 and 49, respectively.

significant difference between the PES(F,Cl) and CCSD(T) geometries. As shown in Table 3, there is also good agreement between the PES(F,Cl) vibrational frequencies and the ab initio and experimental[48,49] values. The comparison in Table 3 is with the CEPA-1 frequencies, since frequencies for only the symmetric modes were determined in the CCSD(T) calculations. However, the CEPA-1 and CCSD(T) symmetric frequencies agree to within 15 cm^{-1}.[42]

III. Classical Trajectory Calculations

The PES(F,Cl) potential energy function and its derivatives with respect to Cartesian coordinates were incorporated into the general chemical dynamics computer program VENUS96,[50] which was used for the classical trajectory simulations. A total of 4000−16 000 trajectories with random initial conditions are used to calculate reaction attributes at a specific relative translational energy and either a specific CH_3Cl vibrational/rotational temperature or for a specific vibrational excitation pattern with a fixed rotational temperature. The number of trajectories calculated depends on the relative translational energy and the temperature. A larger number of trajectories are calculated for higher temperature and/or higher relative translational energy to ensure a constant uncertainty in the trajectory rate constant. The estimated absolute uncertainty of the calculated rate constants is within 10%.[34] The relative uncertainty is within 5%.

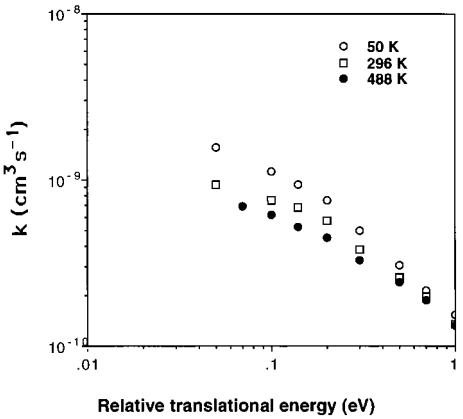

Figure 1. Trajectory rate constants for $F^- + CH_3Cl \rightarrow FCH_3 + Cl^-$ versus E_{rel} and CH_3Cl temperature.

A polyatomic quasiclassical sampling method, a standard option in VENUS96 and described previously,[51,52] was used to choose initial conditions for CH_3Cl. To create a thermal vibrational energy distribution for CH_3Cl, quantum numbers for the normal modes of vibration are chosen by sampling the quantum harmonic oscillator probability distributions. Random phases are then selected for the normal mode vibrations to transform the quantum numbers to normal mode coordinates and momenta. The total angular momentum of CH_3Cl and its components are chosen by sampling the classical rotational energy probability distribution for a symmetric top.[52] The normal mode momenta and coordinates and rotational angular momentum components are then transformed to Cartesian coordinates and momenta, which are used for integrating the classical equations of motion. CH_3Cl is then randomly rotated about its Euler angles so that it has a random orientation with respect to F^-.

The trajectories are begun at a 40 Å ion−molecule separation. For each temperature and relative translational energy, the impact parameter b is selected from a uniform random distribution between zero and a maximum value b_{max}. The value of b_{max} is determined by gradually increasing b until no reaction occurs for at least 500 trajectories at that impact parameter. The reaction rate constant at a relative translational energy E_{rel} is given by

$$k(E_{rel}) = 2\pi\sqrt{\frac{2E_{rel}}{\mu}}\int\chi(p,q)b\,db \qquad (6)$$

where μ is the reduced mass of the ion−molecule partners and $\chi(p,q)$ is the characteristic function with a value of either 1 or 0 for reactive or nonreactive trajectories, respectively.

IV. Results and Discussion

A. Reaction Rate Constant. *1. CH_3Cl Thermal Excitation.* Rate constants for reactions 2 are calculated as a function of relative translational energy at 50, 296, and 488 K CH_3Cl internal temperatures. The results are shown in Figure 1. Figure 2 compares the trajectory and experimental[4] results at 296 and 488 K. Capture collision rate constants[46] are included in Figure 2 for comparison. The trajectory rate constants are in overall agreement with the experimental results—within the combined

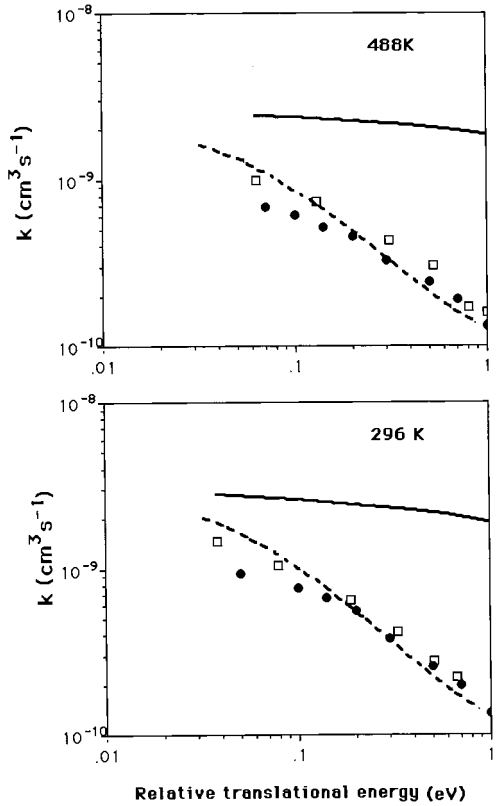

Figure 2. Comparison of trajectory (●), experimental (□), ion−molecule capture (—), and ion−molecule capture/RRKM statistical theory (- - -) rate constants for CH_3Cl temperatures of 296 and 488 K.

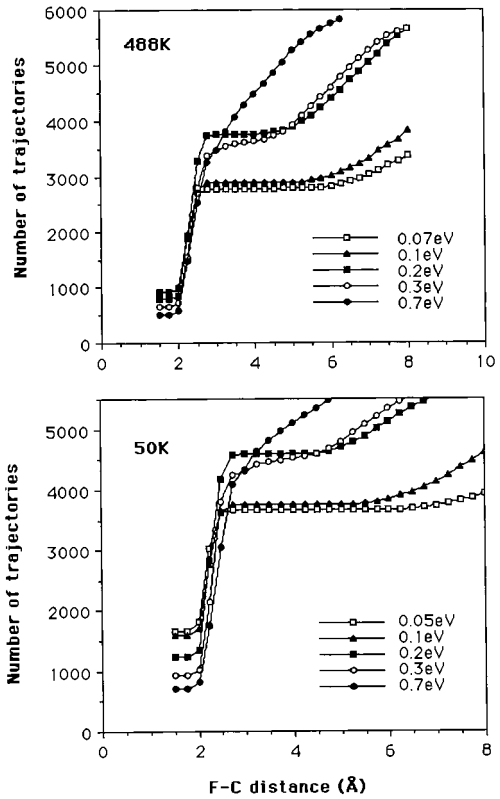

Figure 3. Number of trajectories that arrive at a particular F−C distance for CH_3Cl temperatures of 50 and 488 K and different E_{rel}.

absolute uncertainty of experiment (30%) and the trajectories (10%). The trajectory calculations, however, appear to predict a somewhat smaller negative E_{rel} dependence.

The trajectory and experimental rate constants are lower than the collision capture rate constant, and the reaction efficiency decreases rapidly with increasing E_{rel}. An important resemblance between the trajectory and experimental rate constants is the existence of a break in the slope at about 0.2 eV which divides the reaction rate constant into low- and high-energy regimes with the high-energy regime having a larger negative E_{rel} dependence. At the low-energy regime, the trajectory E_{rel} dependencies at 269 and 488 K are $E_{rel}^{-0.3}$ and $E_{rel}^{-0.4}$, respectively. At high energies, the respective E_{rel} dependencies at these temperatures are $E_{rel}^{-0.9}$ and $E_{rel}^{-0.7}$. Experimental E_{rel} dependencies are $E_{rel}^{-0.5}$ and $E_{rel}^{-1.0}$ for the low and high energies, assuming that the low- and high-energy portions of the combined data of both temperatures can each be fit by a single line. This was justified within the experimental uncertainty of the data. The experimental data appear to show a slight negative dependence on the internal temperature. However, the temperature range studied is not large enough to show a significant temperature dependence. Another resemblance between the experimental and trajectory results is that, at higher relative translational energies, the rate constant appears to be less sensitive to temperature.

Su et al.[4] provided a simple explanation for the change in slope by comparing the capture radius with the average hard-sphere diameter of the ion−molecule system. At low energies, the capture radius is large. The system enters the capture radius before the collision occurs, forming a relatively long-lived ion−molecule intermolecular complex in which the ion−molecule pair has time to rearrange to a favorable collision orientation. At high E_{rel}, the capture radius becomes smaller than the hard-sphere radius, and a capture phenomenon does not take place. Thus, at low energies, the reaction rate constant is controlled partly by the capture rate constant.

The capture phenomenon is studied by observing the number of trajectories that reach a certain ion−molecule separation. Figure 3 shows the number of trajectories (out of 6000) that arrive at various F−C distances at several relative translational energies for 50 and 488 K. For relative translational energies at the low-energy regime (≤ 0.2 eV)), the curves reach a broad plateau before a rapid drop off at a F−C distance of about 2.3 Å. This zero slope region indicates a capture phenomenon. That is, when the ion−molecule partners enter the capture distance, they continue to approach each other until their electron clouds begin to interact. The sudden decrease of the number of trajectories at a 2.3 Å F−C distance reflects the beginning of the electron−electron interaction between the ion−molecule partners. This distance, assuming more or less a backside, rear attack (see section D), corresponds to an ion−molecule center-of-mass separation approximately equal to the average hard-sphere diameter (3.4 Å). For relative translational energies larger than 0.2 eV, no zero slope region is observed, indicating the absence of a capture phenomenon. This is consistent with the reasoning of Su et al.[4]

Figure 3 shows that a larger fraction of the trajectories reach an intermediate separation of 6−8 Å as E_{rel} is increased. This is because the probability of a particular impact parameter b is proportional to b, and the maximum impact parameter b_{max}, leading to reaction, decreases as E_{rel} is increased. At E_{rel} = 0.05 eV b_{max} = 15 Å, and most of the trajectories have values for b considerably larger than 6−8 Å. They can acquire a separation of 6−8 Å if they feel the attractive $F^- + CH_3Cl$ ion−dipole interaction, but many feel a repulsive interaction instead and do not acquire such a close separation. At the much higher E_{rel} of 0.7 eV b_{max} is 6.3 Å, and in the absence of a $F^- + CH_3Cl$ interaction, all trajectories acquire a separation of 6.3

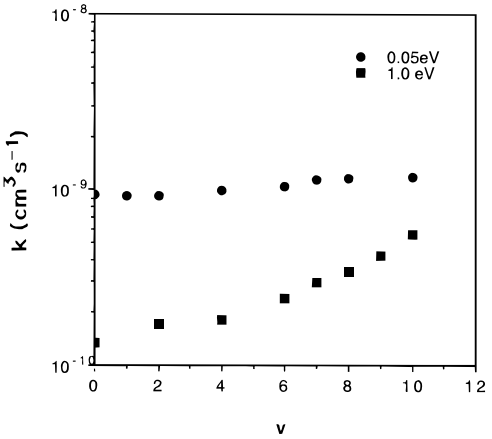

Figure 4. Reaction rate constant vs number of quanta, v, in the A_1 C−Cl stretch mode of CH_3Cl at a 296 K rotational, temperature. E_{rel} = 0.05 and 1.0 eV.

Å or less. Though the vast majority of the E_{rel} = 0.7 eV trajectories do not react, nearly all reach a separation of 6−8 Å before they are deflected.

2. CH_3Cl Mode Specific Excitation. A set of calculations at E_{rel} of 0.05 and 1.0 eV and a CH_3Cl rotational temperature of 296 K, with increasing quanta in the A_1 C−Cl stretch mode of CH_3Cl, were performed to determine the dependence of the S_N2 rate constant on C−Cl stretch excitation. Zero-point energy was added to the remaining modes. The resulting rate constants are presented in Figure 4. At $v = 0$, the rate constants for both E_{rel} values are the same as those determined with a 296 K thermal vibrational distribution for CH_3Cl. This is expected since at 296 K most of the vibrational population is in the v = 0 level for each mode. The relative populations of the C−Cl stretch $v = 1$ and $v = 0$ levels is 0.025 at 296 K.

Before discussing these results, it is useful to consider what the statistical theory calculation of ref 40 predicts for the effect of v on the S_N2 rate constant. For a low E_{rel} of 0.5 eV there is a resulting small rotational energy at the low central barrier, and the effect of increasing the CH_3Cl energy (e.g., v) is to increase the probability the F^-- - -CH_3Cl complex dissociates back to the reactants. Thus, increasing v is predicted to decrease the reaction rate. In particular, for $v = 0$, 1, 2, 3, 5, and 10 the relative S_N2 rate constants are 1.00, 0.72, 0.56, 0.46, 0.35, and 0.24. In contrast, for the much larger E_{rel} of 1.0 eV there is a resulting larger rotational energy at the central barrier. This effect and the increased excitation of the F^-- - - CH_3Cl complex make dissociation of the complex to form the $F^- + CH_3Cl$ reactants competitive with that for forming the $FCH_3 + Cl^-$ products. As a result, for E_{rel} = 1.0 eV the S_N2 rate constant slightly increases by a factor 1.07 in increasing v from 0 to 10.

With increasing number of quanta in the C−Cl stretch mode, the trajectory rate constant at E_{rel} = 0.05 eV appears to stay quite constant, showing only a slight increase with $v > 4$. At E_{rel} = 1.0 eV, on the other hand, the rate constant significantly increases with increasing quanta in the C−Cl stretch mode, approaching the E_{rel} = 0.05 eV rate constant. These results are significantly different from the predictions of the statistical theory calculations. At low E_{rel}, the reaction rate is controlled partially by the capture process, but because of the nonstatistical and direct nature of the ensuing reaction, an increase of reactant vibrational energy leads to a small effect on the reaction rate constant. At high E_{rel}, however, the reaction is more direct without capture, and excitation of the C−Cl stretch has a pronounced effect on the reaction probability.

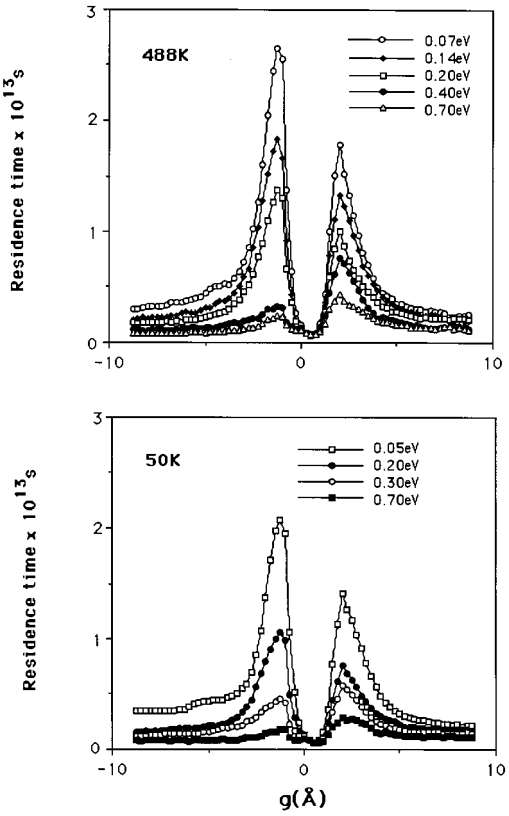

Figure 5. Plots of the average residence time versus $g = (r_{C-Cl} - r_{C-F})$ for reactive trajectories with CH_3Cl temperatures of 50 and 488 K and different E_{rel}.

3. Comparison with Statistical Ion−Molecule Capture/RRKM Calculations. In previous work,[40] an ion−molecule capture/RRKM statistical model was used to calculate the $F^- + CH_3Cl$ S_N2 rate constant versus E_{rel} and CH_3Cl temperature. These rate constants are plotted in Figure 2, where they are compared with the trajectory rate constants reported here. The PES(F,Cl) potential energy function was used for both sets of calculations. Overall, there is good agreement between the trajectory and statistical theory rate constants. However, there are some differences at low and high E_{rel}. At low E_{rel} the statistical theory rate constants are somewhat higher, while they are slightly lower at high E_{rel}. Both the trajectory and statistical theory calculations show that the rate constant is less sensitive to temperature at high E_{rel}.

B. Complex Lifetime. An estimation of the average lifetimes of the intermediate complexes was made by studying the average residence time $\bar{t}(g)$ of reactive trajectories as a function of the extent of reaction $g = (r_{C-Cl} - r_{C-F})$. The average lifetime $\langle t \rangle$ is related to $\bar{t}(g)$ by

$$\langle t \rangle = \int_{g_{min}}^{g_{max}} \bar{t}(g)\, dg \qquad (7)$$

where g_{min} and g_{max} identify the range of g which defines the complex. Plots of the average residence time for reactive trajectories, versus g with 0.125 Å intervals, are given in Figure 5 for CH_3Cl temperatures of 50 and 488 K and several different relative translational energies. The value of each point represents the average amount of time that a trajectory spends within the corresponding g interval. These plots show the existence of complexes on the reactant side (F^-- - -CH_3Cl) and the product side (FCH_3- - -Cl^-) separated by the central potential barrier. The average lifetimes of the complexes are estimated from the area under the peaks, and the values are plotted in Figure 6.

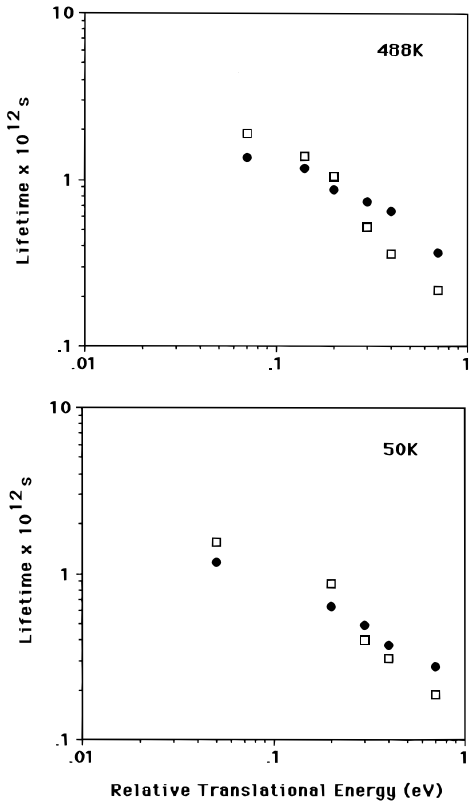

Figure 6. Average lifetimes of reactant F^-- - -CH_3Cl complex (□) and product FCH_3- - -Cl^- complex (●) for CH_3Cl internal temperatures of 50 and 488 K and different E_{rel}.

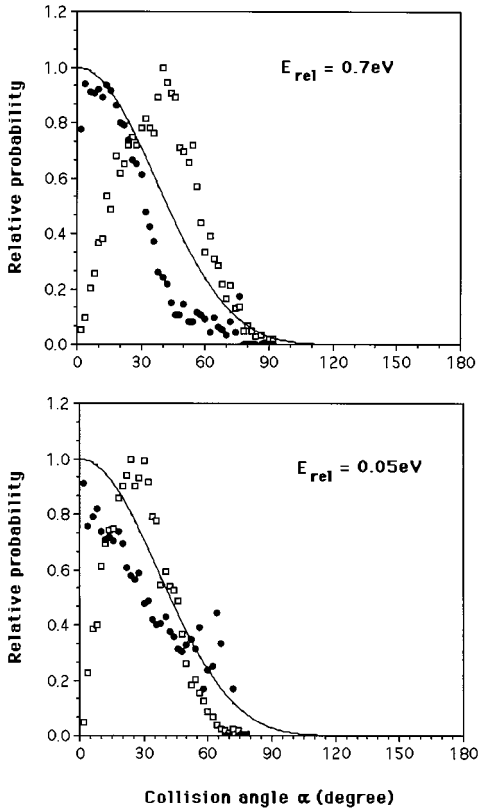

Figure 7. Dynamical stereochemistry for a CH_3Cl temperature of 50 K: □, probability of a displacement α of the F---C−Cl angle from 180° when the trajectories reaches the hard-sphere diameter of 3.4 Å; ●, fraction of trajectories that react which obtain the particular value of α; and (—) plot of eq 5 with $n = 26$ (ref 4) and θ converted to α.

The lifetimes decrease from about 1 ps at low E_{rel} to about 0.1 ps at high E_{rel}. Studies of the extent of IVR in ion−molecule complexes versus lifetimes of the complexes[53] indicate the lifetimes of these F^-- - -CH_3Cl and FCH_3- - -Cl^- complexes are too short for complete energy randomization to occur. Partial energy randomization may take place at the low-energy regime.

At the low-energy regime ($E_{rel} \leq 0.2$ eV), the lifetime of the complex on the reactant side is longer than that on the product side. On the other hand, at the high-energy regime, the lifetime of the complex on the reactant side is shorter than that on the product side. Note that the complex lifetime on the reactant side drops suddenly at $E_{rel} > 0.2$ eV, while the complex lifetime on the product side decreases gradually as E_{rel} increases. This observation further reveals the different reaction dynamics between the low- and the high-energy regimes. At low translational energies a capture complex is formed, resulting in a relatively long-lived ion−molecule complex on the reactant side. At high translational energies, the reaction is more direct, and the capture phenomenon does not occur which leads to a relatively short complex lifetime. The complex lifetimes are rather insensitive to the CH_3Cl temperature.

C. Central Barrier Recrossing. The difference between the high- and low-energy regimes is further demonstrated by the trajectories that recross the central barrier. The fraction of trajectories that recross the central barrier is about 10% in all cases. At low relative translational energies, the majority of recrossing trajectories result in products. On the other hand, at high energies, most of the recrossing trajectories return back to reactants. For a CH_3Cl temperature of 50 K, 66, 54, 34, and 32% of the recrossing trajectories react at E_{rel} of 0.05, 0.20, 0.50, and 1.0 eV, respectively. When the temperature is increased to 488 K, 61, 59, 46, and 24% of the recrossing trajectories react at E_{rel} of 0.07, 0.20, 0.30, and 1.00 eV, respectively.

Because of the high barrier and tight transition-state structure for the FCH_3- - -$Cl^- \rightarrow F^-$- - - CH_3Cl process compared to FCH_3- - -$Cl^- \rightarrow FCH_3 + Cl^-$, RRKM theory predicts a negligibly small amount of barrier recrossing for each of the energies considered in this work. The observed recrossings arise from nonstatistical effects.

D. Dynamical Stereochemistry. The dynamical stereochemistry[29] of the collisions and reactive events was studied by observing the displacement α of the F- - -C−Cl angle from 180°, when a trajectory reached the average hard-sphere diameter of 3.4 Å. The relative number of trajectories that obtain a specific α is given by the open squares in Figure 7 for calculations with a CH_3Cl temperature of 50 K and E_{rel} of 0.05 and 0.7 eV. Most of the collisions occur at α less than 60°, indicating that the ion−molecule partners orient themselves to a rear attack position upon collision. The solid circles are the fraction of trajectories at the corresponding collision angle that lead to reaction. This fraction is a measure of the reaction probability at that collision angle. The trajectory reaction probability may be compared with the empirical probability function $P(\theta)$ in eq 5, where θ is the angle between the C−Cl bond and the line joining the centers of mass of F^- and CH_3Cl. The solid lines in Figure 7 are plots of eq 5 with θ converted to α and n set to 26 to match the fit to experiment.[4] At both low and high relative translational energies, the trajectory collision angle dependent reaction probability is generally lower than the simple empirical function of eq 5. While the collision angle distribution shifts to large angles at higher E_{rel}, the reaction probability function appears to shift to smaller angles and becomes narrower at higher energies. As a consequence, most of the collisions at high E_{rel} occur at angles with low reaction probability. This may be one of the reasons for the rather rapid

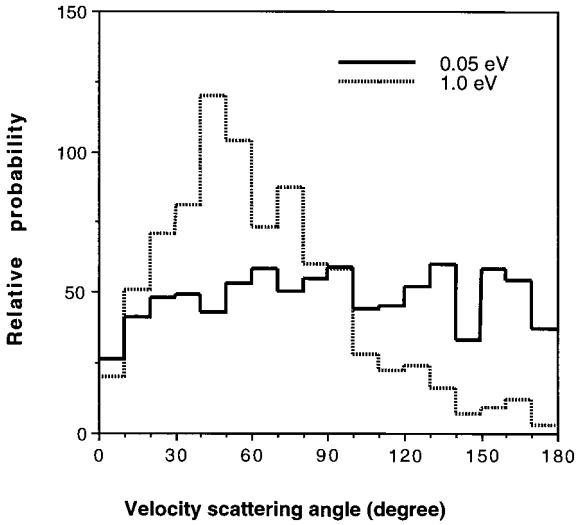

Figure 8. Velocity scattering angle distribution at $E_{rel} = 0.05$ and 1.0 eV.

decrease of the reaction efficiency as E_{rel} increases. The above results indicate that the collision angle dependent reaction efficiency cannot be accurately described by a function of the collision angle alone. Rather, the angle dependent probability function changes as the relative translational energy changes. A similar phenomenon is observed at other temperatures.

E. Velocity Scattering Angle. The distribution of the angle between the initial and final relative velocity vectors was calculated at $E_{rel} = 0.05$ and 1.0 eV, and the results are shown in Figure 8. If the scattering angle is zero, there is forward scattering, and the CH_3F product scatters in the same direction as the initial relative velocity. For a scattering angle of π, the scattering is backward with the direction of the relative velocity vector reversed. Figure 8 shows that at low E_{rel} the scattering angle distribution is isotropic, suggesting that a relatively long-lived complex is formed with partial energy randomization.[54] At $E_{rel} = 1.0$ eV, however, most of the product molecules are forward scattered with an angle less than 90°, suggesting a more direct reaction with a short complex lifetime.

F. Product Energy and Angular Momentum Distributions. *1. Effect of Reagent Vibrational Energy.* Product energy and angular momentum distributions were calculated with 0, 2, and 7 quanta in the C−Cl stretch mode of CH_3Cl, zero-point energy in the remaining modes, a 296 K CH_3Cl rotational temperature, and a reactant E_{rel} of 0.05 eV. The resulting distributions are shown in Figures 9 and 10. The averages of the distributions are given in Table 4. The product energy partitioning without C−Cl stretch excitation disagrees with the previous experimental study of Van Orden et al.,[9] which indicated the majority of the products are formed with less than 20% of the available energy in CH_3Cl rotation and vibration. Here it is found that, for thermal reactant conditions, on average 76% of the available energy goes to CH_3Cl rotation and vibration. Increasing the reactant C−Cl stretch vibrational energy has a significant positive effect on the product vibrational energy, but has small effects on the product rotational and relative translational energies and product rotational and orbital angular momenta. The C−Cl stretch excitation is almost exclusively transferred to vibrational energy of the product CH_3F. For $v = 0$, the calculated average product vibrational energy is 22.3 kcal/mol. At $v = 7$, the energy of the C−Cl stretch mode is about 15 kcal/mol above the ground state. At this vibrational excitation, the calculated average product vibrational energy is 36.2 kcal/mol, 13.9 kcal/mol higher than that at $v = 0$.

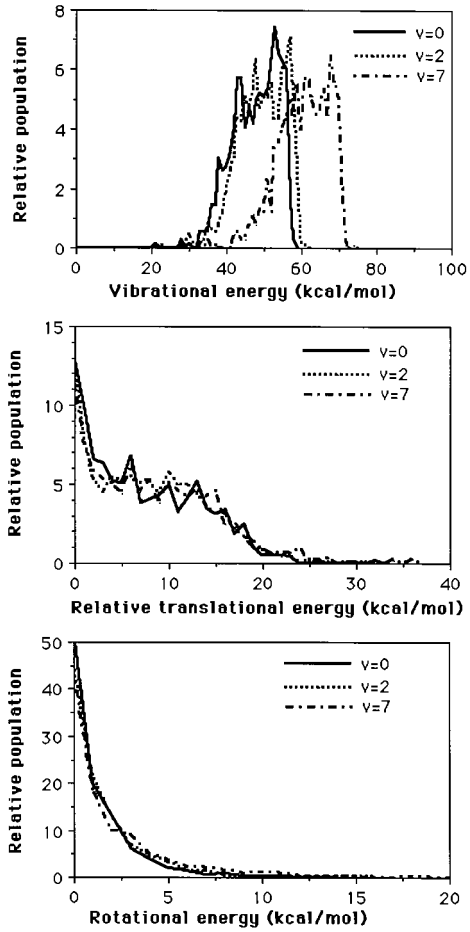

Figure 9. Product vibrational, relative translational, and rotational energy distributions (plotted in 1.0 kcal/mol intervals) for different reactant C−Cl stretch states. $E_{rel} = 0.05$ eV and the CH_3Cl temperature is 296 K. The vibrational energy is with respect to the classical potential energy minimum.

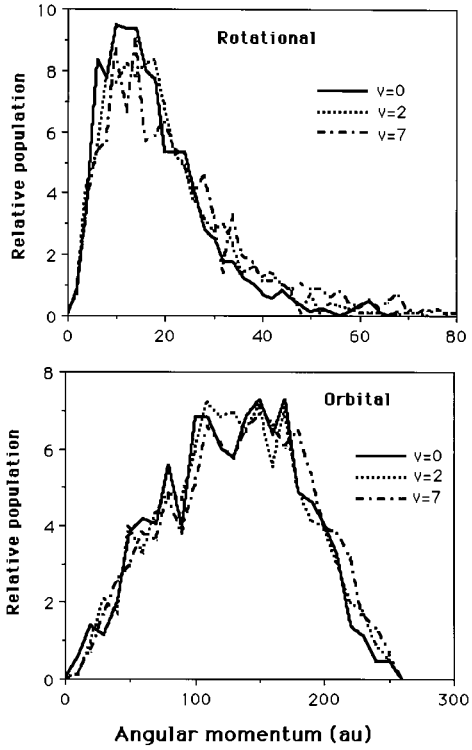

Figure 10. Distributions of product rotational and orbital angular momentum in units of $\hbar$. Reactant conditions are the same as in Figure 9.

TABLE 4: Average Product Energies and Angular Momenta

reactant conditions[a]		product properties[b]					
E_{rel}	v_{C-Cl}	$\langle E_{rel}\rangle$	$\langle E_{rot}\rangle$	$\langle E_{vib}\rangle$	$\langle J\rangle$	$\langle l\rangle$	$\langle j\rangle$
0.05	0	7.7	1.7	22.3	129	127	17.2
0.05	2	8.2	1.8	26.1	132	128	18.9
0.05	7	8.6	2.2	36.2	137	134	21.7
0.70	0	25.8	2.5	18.4	153	139	23.6

[a] The CH_3Cl temperature is 296 K. The reactant relative translational energy is in electronvolts, and v_{C-Cl} is the number of quanta in the C−Cl stretch mode. Zero-point energy is in the remaining modes. [b] The average product energies are in kcal/mol, and the angular momenta are given in units of $\hbar$. *J*, *l*, and *j* are the total, orbital, and CH_3F rotational angular momentum, respectively. The CH_3F zero-point energy is subtracted from the product vibrational energy.

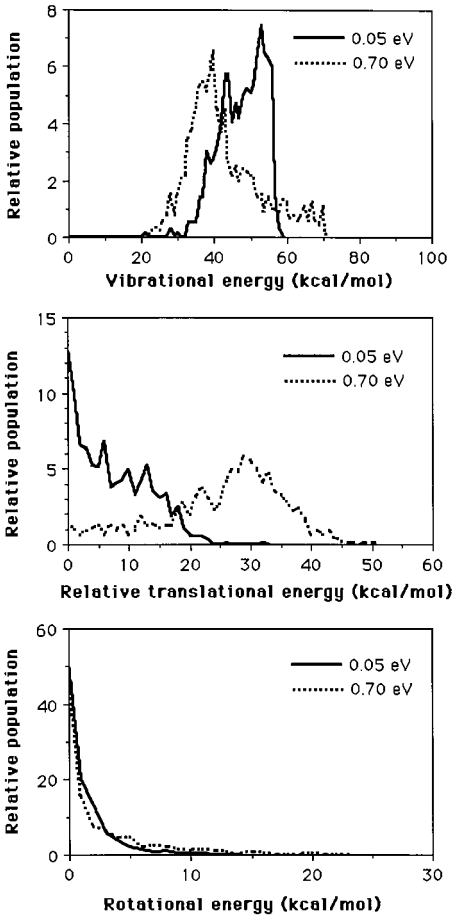

Figure 11. Product energies as in Figure 9, but comparison of different reactant conditions with zero quanta in the C−Cl stretch, 296 K CH_3Cl temperature, and E_{rel} of 0.05 and 0.70 eV.

2. Effect of Reactant Relative Translational Energy. Product energy and angular momentum distributions were also calculated at $E_{rel} = 0.70$ eV, while setting the reactant vibrational modes in their zero-point levels and adding a 296 K rotational temperature to CH_3Cl, to compare with the above $E_{rel} = 0.05$ eV calculations. The results are shown in Figure 11 and Table 4. There is a large shift in the product relative translational energy (i.e., a 18 kcal/mol increase in average energy) upon increasing E_{rel} from 0.05 to 0.7 eV (i.e., 15 kcal/mol). The product vibrational energy distribution is broadened, and the average product vibrational energy decreases by 3.9 kcal/mol. It is 22.3 and 18.4 kcal/mol at E_{rel} of 0.05 and 0.7 eV, respectively. Only small positive shifts are observed in the product rotational energy and rotational and orbital angular

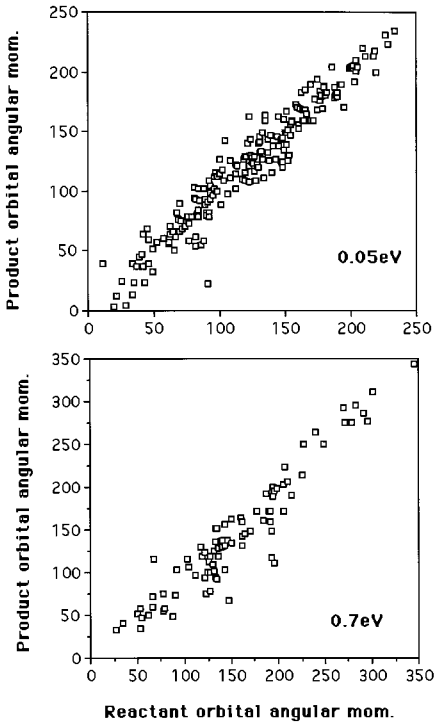

Figure 12. Plots of product versus reactant orbital angular momentum for E_{rel} of 0.05 and 0.7 eV, with CH_3Cl zero-point vibrational energy and 296 K rotational temperature.

momentum distributions. In particular, the angular momentum distributions are very similar to those plotted in Figure 10, with slight shifting to higher values (see Table 4). These results imply that essentially all of the relative translational energy of the reactants is transferred to relative motion of the products and has only small effects on other product properties.

The above results indicate that the exothermicity of reaction 2 is primarily partitioned to product vibration and excess reactant energy is nonstatistically partitioned to the products by vibration to vibration (V → V) and translation to translation (T → T) energy transfer processes. These results suggest that the intramolecular vibrational modes of CH_3Cl are weakly coupled to the relative motion of the reactant ion−molecule pair, which is consistent with previous trajectory studies of S_N2 reactions.[32,33] It was shown that for S_N2 reactions, complexes are formed by T → R energy transfer in which the relative translational energy is transferred to rotational motion of the complex. Since most reactive trajectories occur at collision angles between 10° and 40° (Figure 7), a significant fraction of the reactant E_{rel} is transferred to the rotational energy of the complex. The observation that a change in E_{rel} affects mainly the product relative translational energy in reaction 2 suggests that the rotational motion of the complex formed by collision is used primarily for spinning off the products CH_3F and Cl, rather than increasing the product rotational energy. Comparison of the reactant and product orbital angular momenta for reactive trajectories shows negligible differences (Figure 12). Individual trajectories show that the average deviation between the product and reactant orbital angular momentum is less than 15%. The correlation coefficient between these orbital angular momenta is 0.93 and 0.90 for E_{rel} of 0.05 and 0.7 eV, respectively. (Similarly, the correlation between the total angular momentum and product orbital angular momentum is 0.95 and 0.94 for E_{rel} of 0.05 and 0.7 eV.) These results are a demonstration of the nonstatistical behavior of the $F^- + CH_3Cl$ reaction system in which the energy of the intermediates is

not completely randomized. Morris and Viggiano[15] studied a series of S_N2 reactions and found that reactions of halide ions with monohalogenated methanes also behave nonstatistically and that vibrational and translational energies have different influences on the reactivity and reaction dynamics.

V. Summary

Rate constants calculated for reaction 2 by the trajectory method are in good agreement with the experimental results.[4] The trajectory rate constants are also in semiquantitative agreement with statistical ion−molecule capture/RRKM calculations.[40]

Results from reactant relative translational energy dependent calculations divide the reaction into low- and high-energy regimes. At low energies, the reaction dynamics is partly controlled by the capture process. The capture phenomenon is demonstrated by observing those trajectories that enter the capture distance. For these trajectories, the ion−molecule pair continue to approach each other until their electron clouds begin to interact. At this energy regime, the reaction rate constant is relatively insensitive to a change in the relative translational energy, the lifetime of the F^-- - -CH_3Cl complex is longer than that of the FCH_3- - -Cl^- complex, and the velocity scattering angle distribution is isotropic. On the other hand, at the high-energy regime the lifetimes of both the F^-- - -CH_3Cl and FCH_3- - -Cl^- complexes are shorter than those at the low-energy regime; with the FCH_3- - -Cl^- now somewhat longer lived, the reaction rate constant decreases more rapidly with increasing relative translational energy, and the velocity scattering angle distribution appears to be anisotropic. For both the low- and high-energy regimes, the reaction probability decreases with increasing α the displacement of the F^-- - -C−Cl angle from π; i.e., trajectories that collide backside along the F^-- - -C−Cl axis have the greatest probability to react. At high relative translational energies, the reaction probability concentrates at smaller α than at low energies, presumably because of the more direct nature of the reaction at high energies. However, at the higher energies $F^- + CH_3Cl$ collisions occur at larger α, since there is less time for orientation of the CH_3Cl dipole to occur. Most of the reactive trajectories occur with α between 10° and 40°.

Exciting the C−Cl stretch mode of CH_3Cl has little effect on the reaction rate and leads almost exclusively to V → V energy transfer to the product molecule CH_3F. Only at high reactant relative translational energies, where the reaction rate is low, does C−Cl excitation lead to a significant increase in the reaction rate constant. The reaction exothermicity is preferentially partitioned to product vibration, in disagreement with a previous experiment.[9] The effect of an increase in the reactant relative translational energy on the product energy partitioning is also quite selective. It mainly results in T → T transfer to product relative translational energy. The angular momentum of the complexes formed by collision is transferred to orbiting motion of the products, resulting in a strong correlation between reactant and product orbital angular momentum. Overall, the reaction system behaves nonstatistically, although at low relative translational energies, partial energy randomization may occur.

Acknowledgment. This research was supported by the National Science Foundation.

References and Notes

(1) Olmstead, W. N.; Brauman, J. I. *J. Am. Chem. Soc*. **1997**, *99*, 4219. Pellerite, M. J.; Brauman, J. I. *J. Am. Chem. Soc.* **1980**, *102*, 5993. Pellerite, M. J.; Brauman, J. I. *J. Am. Chem. Soc.* **1983**, *105*, 2672.

(2) Caldwell, G.; Magnera, T. F.; Kebarle, P. J. *J. Am. Chem. Soc*. **1984**, *106*, 949.

(3) Dodd, J. A.; Brauman, J. I. *J. Am. Chem. Soc*. **1984**, *106*, 5356. Dodd, J. A.; Brauman, J. I. *J. Phys. Chem.* **1986**, *90*, 3559.

(4) Su, T.; Morris, R. A.; Viggiano, A. A.; Paulson, J. F. *J. Phys. Chem*. **1990**, *94*, 8426.

(5) Barlow, S. E.; Van Doren, J. M.; Bierbaum, V. M. *J. Am. Chem. Soc*. **1988**, *110*, 7240.

(6) Viggiano, A. A.; Paschkewitz, J. S.; Morris, R. A.; Paulson, J. F.; Gonzalez-Lafont, A.; Truhlar, D. G. *J. Am. Chem. Soc*. **1991**, *113*, 9404.

(7) (a) DePuy, C. H.; Gronert, S.; Mullin, A.; Bierbaum, V. M. *J. Am. Chem. Soc*. **1990**, *112*, 8650. (b) Gronert, S.; DePuy, C. H.; Bierbaum, V. M. *J. Am. Chem. Soc*. **1991**, *113*, 4009.

(8) (a) Graul, S. T.; Bowers, M. T. *J. Am. Chem. Soc*. **1991**, *113*, 9696. (b) Graul, S. T.; Bowers, M. T. *J. Am. Chem. Soc*. **1994**, *116*, 3875.

(9) Van Orden, S. L.; Pope, R. M.; Buckner, S. W. *Org. Mass Spectrom.* **1991**, *26*, 1003.

(10) Cyr, D. M.; Posey, L. A.; Bishea, G. A.; Han, C.-C.; Johnson, M. A. *J. Am. Chem. Soc*. **1991**, *113*, 9697.

(11) Cyr, D. M.; Bishea, G. A.; Scarton, M. G.; Johnson, M. A. *J. Chem. Phys*. **1992**, *97*, 5911.

(12) Giles, K.; Grimsrud, E. P. *J. Phys. Chem*. **1992**, *96*, 6680. Knighton, W. B.; Boghar, J. A.; O'Connor, P. M.; Grimsrud, E. P. *J. Am. Chem. Soc*. **1993**, *115*, 12079. Sahlstrom, K. E.; Knighton, W. B.; Grimsrud, E. P. *J. Phys. Chem. A* **1997**, *101*, 1501.

(13) Viggiano, A. A.; Morris, R. A.; Paschkewitz, J. S.; Paulson, J. F. *J. Am. Chem. Soc*. **1992**, *114*, 10477.

(14) Wladkowski, B. D.; Lim, K. F.; Allen, W. D.; Brauman, J. I. *J. Am. Chem. Soc*. **1992**, *114*, 9136. Viggiano, A. A.; Morris, R. A.; Su, T.; Wladkowski, B. D.; Craig, S. L.; Zhong, M.; Brauman, J. I. *J. Am. Chem. Soc*. **1994**, *116*, 2213. Craig, S. L.; Brauman, J. I. *Science* **1997**, *276*, 1536.

(15) Viggiano, A. A.; Morris, R. A. *J. Phys. Chem.* **1994**, *98*, 3740.

(16) O'Hair, R. A. J.; Davico, G. E.; Hacaloglu, J.; Dang, T. T.; DePuy, C. H.; Bierbaum, V. *J. Am. Chem. Soc*. **1994**, *116*, 3609.

(17) Li, C.; Ross, P.; Szulejko, J. E.; McMahon, T. B. *J. Am. Chem. Soc.* **1996**, *118*, 9360.

(18) Craig, S. L.; Brauman, J. I. *J. Phys. Chem. A* **1997**, *101*, 4745.

(19) DeTuri, V. F.; Hintz, P. A.; Ervin, K. M. *J. Phys. Chem. A* **1997**, *101*, 5969.

(20) Seeley, J. V.; Morris, R. A.; Viggiano, A. A.; Wang, H.; Hase, W. L. *J. Am. Chem. Soc*. **1997**, *119*, 577.

(21) Le Garrec, J.-L.; Rowe, B. R.; Queffelec, J. L.; Mitchell, J. B. A.; Clary, D. C. *J. Chem. Phys*. **1997**, *107*, 1021.

(22) Chabinyc, M. L.; Craig, S. L.; Regan, C. K.; Brauman, J. I. *Science* **1998**, *279*, 1882.

(23) Basilevsky, M. V.; Ryaboy, V. M. *Chem. Phys. Lett*. **1986**, *129*, 71. Ryaboy, V. M. *Chem. Phys. Lett*. **1989**, *159*, 371. Ryaboy, V. M. In *Advances in Classical Trajectory Methods*; Hase, W. L., Ed.; JAI Press: Greenwich, CT, 1994; Vol. 2, pp 115−145.

(24) Vande Linde, S. R.; Hase, W. L. *J. Am. Chem. Soc*. **1989**, *111*, 2349. Vande Linde, S. R.; Hase, W. L. *J. Phys. Chem*. **1990**, *94*, 6148; Vande Linde, S. R.; Hase, W. L. *J. Chem. Phys*. **1990**, *93*, 7962. Peslherbe, G. H.; Wang, H.; Hase, W. L. *J. Chem. Phys*. **1995**, *102*, 5626.

(25) Vande Linde, S. R.; Hase, W. L. *J. Phys. Chem.* **1990**, *94*, 2778.

(26) Tucker, S. C.; Truhlar, D. G. *J. Phys. Chem*. **1989**, *93*, 8138. Tucker, S. C.; Truhlar, D. G. *J. Am. Chem. Soc*. **1990**, *112*, 3338.

(27) Cho, Y. J.; Vande Linde, S. R.; Zhu, L.; Hase, W. L. *J. Chem. Phys*. **1992**, *96*, 8275.

(28) Billing, G. D. *Chem. Phys*. **1992**, *159*, 109.

(29) Hase, W. L.; Cho, Y. J. *J. Chem. Phys*. **1993**, *98*, 8626.

(30) Wang, H.; Peslherbe, G. H.; Hase, W. L. *J. Am. Chem. Soc*. **1994**, *116*, 9644. Peslherbe, G. H.; Wang, H.; Hase, W. L. *J. Am. Chem. Soc*. **1996**, *118*, 2257.

(31) Wladkowski, B. D.; Allen, W. D.; Brauman, J. I. *J. Phys. Chem*. **1994**, *98*, 13532.

(32) Hase, W. L. *Science* **1994**, *266*, 998.

(33) Wang, H.; Zhu, L.; Hase, W. L. *J. Phys. Chem*. **1994**, *98*, 1608. Wang, H.; Hase, W. L. *J. Am. Chem. Soc*. **1995**, *117*, 9347.

(34) Hu, W.-P.; Truhlar, D. G. *J. Am. Chem. Soc*. **1995**, *117*, 10726.

(35) (a) Glukhovtsev, M. N.; Pross, A.; Radom, L. *J. Am. Chem. Soc*. **1995**, *117*, 2024. (b) *J. Am. Chem. Soc.* **1996**, *118*, 6273.

(36) Seeger, S. Dissertation, Cuvillier Verlag, Göttingen, 1995.

(37) Wang, H.; Hase, W. L. *Chem. Phys*. **1996**, *212*, 247.

(38) Clary, D. C.; Palma, J. *J. Chem. Phys*. **1996**, *106*, 575.

(39) Wang, H.; Goldfield, E. M.; Hase, W. L. *J. Chem. Soc., Faraday Trans*. **1997**, *93*, 737.

(40) Wang, H.; Hase, W. L. *J. Am. Chem. Soc*. **1997**, *119*, 3093.

(41) Wang, H. Hase, W. L. *Int. J. Mass Spectrom. Ion Processes* **1997**, *167/168*, 573.

(42) Botschwina, P.; Horn, M.; Seeger, S.; Oswald, R. *Ber. Bunsen-Ges. Phys. Chem*. **1997**, *101*, 387.

(43) Baer, T.; Hase, W. L. In *Unimolecular Reaction Dynamics−Theory and Experiments*; Oxford: New York, 1996.

(44) Glasstone, S.; Laidler, K. J.; Eyring, H. In *The Theory of Rate Processes*; McGraw-Hill: New York, 1941.

(45) Lias, S. G.; Bartmess, J. E.; Liebmann, J. F.; Holmes, J. L.; Levin, R. D.; Mallard, W. G. *J. Phys. Chem. Ref. Data* **1988**, *17* (Suppl. 1). Zero-point and thermal energy differences between reactants and products for reaction 2 are very small.

(46) Su, T.; Chesnavich, W. J. *J. Chem. Phys.* **1982**, *76*, 5183. Su, T. *J. Chem. Phys.* **1994**, *100*, 4703.

(47) Troe, J. *J. Chem. Phys*. **1996**, *105*, 6249.

(48) Law, M. M.; Duncan, J. L.; Mills, I. M. *J. Mol. Spectrosc.* **1992**, *260*, 323.

(49) Duncan, J. L.; Law, M. M. *J. Mol. Spectrosc.* **1990**, *140*, 13.

(50) Hase, W. L.; Duchovic, R. J.; Hu, X.; Komornicki, A.; Lim, K. F.; Lu, D.-h.; Peslherbe, G. H.; Swamy, K. N.; Vande Linde, S. R.; Varandas, A.; Wang, H.; Wolf, R. J. *QCPE* **1996**, *16*, 671.

(51) Chapman, S.; Bunker, D. L. *J. Chem. Phys*. **1975**, *62*, 2890. Sloane, C. S.; Hase, W. L. *J. Chem. Phys*. **1977**, *66*, 1523. Hase, W. L.; Ludlow, D. M.; Wolf, R. J.; Schlick, T. *J. Phys. Chem*. **1981**, *85*, 958.

(52) Bunker, D. L.; Goring Simpson, E. A. *Faraday Discuss. Chem. Soc*. **1973**, *55*, 93.

(53) Boering, K. A.; Brauman, J. A. *J. Chem. Phys*. **1992**, *97*, 5439.

(54) Levine, R. D.; Bernstein, R. B. *Molecular Reaction Dynamics and Chemical Reactivity*; Oxford: New York, 1987.